# Closed-form expressions for state-to-state charge-transfer differential cross sections in a modified Faddeev three-body approach

E. Ghanbari Adivi,[1] M. J. Brunger,[2] M. A. Bolorizadeh,[3,*] and L. Campbell[2]
[1]*Physics Department, Yazd University, Yazd, Iran*
[2]*ARC Centre of Excellence for Antimatter-Matter Studies, SoCPES, Flinders University, SA, Australia*
[3]*ICST, Mahan, Iran and Physics Department, Shahid Bahonar University of Kerman, Kerman, Iran*
(Received 28 June 2006; published 6 February 2007)

The second-order Faddeev-Watson-Lovelace approximation in a modified form is applied to charge transfer from hydrogenlike target atoms by a fully stripped energetic projectile ion. The state-to-state, $nlm \rightarrow n'l'm'$, partial transition amplitudes are calculated analytically. The method is specifically applied to the collision of protons with hydrogen atoms, where differential cross sections of different transitions are calculated for incident energies of 2.8 and 5.0 MeV. It is shown that the Thomas peak is present in all transition cross sections. The partial cross sections are then summed and compared with the available forward-angle experimental data, showing good agreement.

DOI: 10.1103/PhysRevA.75.022704 PACS number(s): 34.70.+e, 34.50.Pi

## I. INTRODUCTION

As charged particles traverse an absorbing medium at high energies, they lose kinetic energy due to elastic, inelastic, rearrangement, and break-up processes. In particular the charge transfer process is responsible for producing a high energy neutral projectile as the particle passes through the medium. As a consequence a knowledge of this process is important in many different areas of science and technology [1,2].

The process in which an energetic projectile ion impinges on a neutral target atom and scatters off, after capturing an electron to form an atom, has been studied for a long time both experimentally and theoretically. Indeed charge transfer to protons by atomic hydrogen, the simplest of the rearrangement processes, drew considerable attention. Various methods were employed to calculate differential cross sections for the charge transfer process in the collision of protons with atomic hydrogen, which is a three-body problem. The continuum distorted wave (CDW) theory [3], the strong-potential Born (SPB) approach [4], the distorted-wave Born (DWB) method [5], and the boundary-corrected first and second-Born (B1B and B2B) approximations [6,7] are just some examples of the theories applied to investigate this process at moderate and high energies. For energetic collisions, an appropriate perturbation method was developed to study the three-body problem in which the Schrödinger equation for the three-body wave functions was converted into appropriate integral equations. These include such examples as the Lippmann-Schwinger equations or distorted wave integral equations [8]. In the CDW approach, which is widely applied to ion-atom collisions, the Coulomb interactions between different fragments in the initial and final states are also taken into account.

A fully quantum mechanical three-body theory, which is specially applicable to the charge transfer process at moderate and high scattering energies, is the Faddeev-Watson-Lovelace (FWL) theory [9–11]. In this formalism, the single non-Fredholmian Lippmann-Schwinger (LS) integral equation is split into three coupled integral equations. The kernel of the resultant set of three coupled integral equations is connected and compact, and therefore the Faddeev equations have unique solutions for reasonable interaction potentials. The Faddeev formalism has been modified for long range Coulomb interactions by several authors [12,13]. At high energies, Alston [13–15] has calculated the $1s \rightarrow 1s$ differential cross sections for charge transfer in proton-hydrogen collisions by means of a second-order FWL scattering formalism. Another version [16] of the FWL theory was applied to evaluate both the total and differential cross sections, for proton-hydrogen $1s \rightarrow 1s$ transitions. Finally we note that a modified second-order FWL formalism, especially designed for charge transfer in the collision of projectile ions with complex atoms, has been derived by Ghanbari, Adivi, and Bolorizadeh [17]. In a recent work, Vinitsky *et al.* [18] conducted numerical calculations of the second Born and the second Born-Faddeev approximations for charge transfer in the collision of a proton with hydrogen atom, under the kinematical conditions of small scattering angles and high impact energies.

Charge transfer cross sections were measured experimentally, for $p$-H collisions, by Vogt *et al.* [19] and Martin *et al.* [20], where the final state of the product was not analyzed. Thus, the differential cross sections were measured for charge transfer into all final states of the scattered bound system. On the other hand, the available theoretical studies only included the charge transfer from $1s$ state of the target hydrogen to the $1s$ state of the product for the $p$-H collision. This is perhaps due to the labor involved in the computation of state-to-state cross sections for charge transfer from a specified initial state, $i \equiv nlm$, of the target, into another specified final state, $f \equiv n'l'm'$, of the projectile atom.

The present work reports analytical expressions for $nlm \rightarrow n'l'm'$ charge transfer differential cross sections, as calculated by means of a second-order approximation of the FWL three-body approach. In the second-order FWL charge transfer amplitude, five terms are present where the first-Born

*Corresponding author. Email address: mabolori@mail.uk.ac.ir

 

amplitude is determined analytically [21]. In addition, a symmetric-impulse approximation is applied to derive a closed-form for the second-order nuclear-electronic amplitude [22]. The rest of the terms are calculated numerically. Note that the numerical routines are computationally expensive and sometimes involve quite large errors. As a consequence we intend to find the exact analytical forms of the first order internuclear, the second-order nuclear-electronic, and the second-order internuclear amplitudes in order to calculate the differential cross sections. In our method Gegenbauer polynomials, which are components of the radial parts of the initial and final wave functions in momentum space, are expanded in terms of the powers of their arguments in an efficient manner. Using the integral representation of the gamma functions and performing the integrals analytically leads to the closed-form expressions of the state-to-state charge transfer amplitudes, in a second-order approximation. In this paper, atomic units are used unless specified otherwise.

The plan of the paper is as follows. A brief outline of the FWL formalism is given in Sec. II, while in Sec. III a closed form for the second-order nuclear-electronic amplitude is derived, as well as the closed-forms of the three internuclear partial amplitudes. Following this, we present results where the calculated differential cross sections are compared with the relevant experimental measurements and other theoretical calculations. Concluding remarks are made in Sec. V. An appendix is also included, in order to keep the paper comprehensive and to introduce the parameters and quantities which appear throughout the manuscript.

## II. THEORY

Consider a three-body scattering process in which a projectile ion $P$ with charge $Z_P$ is incident on a two-body bounded subsystem composed of an electron $e$ and a target ion $T$ with charge $Z_T$. At sufficiently high impact energies, the collision of the projectile and target results in each of the three possible exit channels (excitation, break-up, or rearrangement) which can be described by an appropriate transition matrix. These transition matrices are expressed in terms of three auxiliary $T$-matrices, $\tau_1$, $\tau_2$, and $\tau_3$, as defined by Newton [23] and reviewed by Chen [24]. An appropriate form of the Faddeev equations governing the set of auxiliary $\tau$ operators is given by;

$$\begin{pmatrix} \tau_1 \\ \tau_2 \\ \tau_3 \end{pmatrix} = \begin{pmatrix} 0 \\ T_{Pe} \\ T_{PT} \end{pmatrix} + \begin{pmatrix} 0 & T_{Te} & T_{Te} \\ T_{Pe} & 0 & T_{Pe} \\ T_{PT} & T_{PT} & 0 \end{pmatrix} G_0^{(+)} \begin{pmatrix} \tau_1 \\ \tau_2 \\ \tau_3 \end{pmatrix} \tag{1}$$

in which $T_{xy}=V_{xy}+V_{xy}G_0^{(+)}T_{xy}$ is the two-body $T$ matrix describing the interaction between particles $x$ and $y$ with mutual interaction potential $V_{xy}$, and $G_0^{(+)}$ is the free three-body Green's function. Zeros along the diagonal of the square matrix remove the self-coupling of the auxiliary operators. This property eliminates the disconnected terms in the kernel of the once-iterated Faddeev equations. For interaction potentials, where there is an absence of the self-coupling terms, this assures the uniqueness of the solution for the Faddeev equations.

Charge transfer is a rearrangement process and the present discussion of the FWL approach concentrates on its transition operator, $\tau_R$, related to the auxiliary $T$ matrices as follows;

$$\tau_R = V_{Pe} + \tau_1 + \tau_3. \tag{2}$$

Equation (1) is usually solved through the Neumann iterative method. By inserting the Neumann expansions for $\tau_1$ and $\tau_3$ into Eq. (2), one derives the Faddeev-Watson multiple scattering expansion [24,25] of the charge transfer process. The expanded form of $\tau_R$ is

$$\tau_R = V_{Pe} + T_{PT} + T_{Te}G_0^{(+)}T_{PT} + T_{Te}G_0^{(+)}T_{Pe} + T_{PT}G_0^{(+)}T_{Pe} + \cdots. \tag{3}$$

Neglecting the higher order terms, the second-order Faddeev amplitude for charge transfer,

$$A_{FWL} = \langle f|\tau_R|i\rangle, \tag{4}$$

is deduced with five partial components. Both the first-Born amplitude, $A_{B1}=\langle f|V_{Pe}|i\rangle$, and the second-order nuclear-electronic amplitude, $A_e^{(2)}=\langle f|T_{Te}G_0^{(+)}T_{Pe}|i\rangle$, arise from the direct transfer of the electron, while the three remaining partial amplitudes, $A_n^{(1)}=\langle f|T_{PT}|i\rangle$, $A_n^{(2a)}=\langle f|T_{Te}G_0^{(+)}T_{PT}|i\rangle$ and $A_n^{(2b)}=\langle f|T_{PT}G_0^{(+)}T_{Pe}|i\rangle$, arise from internuclear scattering. The most general integral forms of the components, participating in the second-order FWL charge transfer amplitude corresponding to the collision of a completely stripped projectile ion with a hydrogenlike target atom, are evaluated elsewhere [15,17,22]. However, the closed forms of these integral expressions will be evaluated and/or discussed in the next section.

## III. AMPLITUDE EVALUATION

### A. The first-Born amplitude; $A_{B1}$

The first-order Born amplitude, $A_{B1}$, is independent of the two-body interaction potential. This amplitude, Eq. (A1) (see Appendix), depends just on the initial and final wave functions denoted by $\varphi_i$ and $\varphi_f$, respectively. The analytical form of the first-Born amplitude is given by [21];

$$\begin{aligned} A_{B1} &= -4\pi^3(K^2 - 2\varepsilon_f)\varphi_f^*(\mathbf{K})\varphi_i(-\mathbf{J}) \\ &= -4\pi^3(J^2 - 2\varepsilon_i)\varphi_f^*(\mathbf{K})\varphi_i(-\mathbf{J}), \end{aligned} \tag{5}$$

where the momentum conservation in the process is $\mathbf{K}+\mathbf{J}+\mathbf{v}=\mathbf{0}$. The quantities not defined throughout the discussions in Sec. III–V are presented in the Table I.

### B. The second-order nuclear-electronic amplitude; $A_e^{(2)}$

The second-order nuclear-electronic amplitude, $A_e^{(2)}=\langle f|T_{Te}G_0^{(+)}T_{Pe}|i\rangle$, is the quantum mechanical description of the Thomas double-scattering mechanism. Classically, the "active" electron is scattered by the target ion after being "kicked off" the hydrogen atom by the projectile in such a manner that the electron finally has almost the same speed and direction as the projectile. These successive collisions

TABLE I. A Table of the parameters used throughout the manuscript.

| Quantity | Definition | Quantity | Definition |
|---|---|---|---|
| $M_T$ | mass of the target | $\rho_{P(T)}$ | $iZ^a_{P(T)}/\mathrm{v}$ |
| $M_P$ | mass of projectile | $\tau$ | $\rho_P+\rho_T$ |
| $\mathbf{k}_i$ | momentum of the initial target electron state | $\gamma(\gamma^a)$ | $iZ_PZ_T/\mathrm{v}(iZ^a_PZ^a_T/\mathrm{v})$ |
| $\mathbf{k}_f$ | momentum of the final projectile electron state | $\delta_{P(T)}$ | $iZ_{P(T)}/\mathrm{v}$ |
| $\varepsilon_i$ | energy of the electron in the initial target state | $\nu^{a(e)}$ | $Z^{a(e)}/\mathrm{v}$ |
| $\varepsilon_f$ | energy of the final electron state | $\sigma^e$ | $\arg\Gamma(1-i\nu^e)$ |
| $Z_T$ | target's charge | $\zeta$ | $\mathrm{v}^2-J^2+2\varepsilon_i$ |
| $Z_P$ | projectile's charge | $a$ | $\zeta/2$ K |
| $Z^a_{P(T)}$ | asymptotic charge of the projectile ($P$) or target ($T$) | $b$ | J/K |
| $Z^e_{P(T)}$ | effective charge of the projectile ($P$) or target ($T$) | $E_i$ | $\frac{1}{2}\mathrm{v}^2-\mathbf{v}\cdot\mathbf{k}_i+\varepsilon_i$ |
| $\mathbf{K}$ | momentum transfer to the target | $E_f$ | $\frac{1}{2}\mathrm{v}^2+\mathbf{v}\cdot\mathbf{k}_f+\varepsilon_f$ |
| $\mathbf{J}$ | momentum transfer to the projectile | $E$ | $\frac{1}{2}\mu_n\mathrm{v}^2$ |
| $\mathbf{v}$ | projectile's velocity | $\mu_n$ | $M_PM_T/(M_P+M_T)$ |

are described by $T$ matrices $T_{Pe}$ and $T_{Te}$, respectively, while the propagation of the electron between the collisions is described by the free Green's function $G_0^{(+)}$. As discussed in the Appendix, the integral form of the second-order nuclear-electronic amplitude is simplified to Eq. (A13). The two inner integrals are Hankel transforms and the outer one is a Fourier transform. The radial part of the initial target state wave function is

$$R_{nl}(k_i)=N_{nl}\frac{k_i^l}{(k_i^2-2\varepsilon_i)^{l+2}}C_{n-l-1}^{l+1}\left(1+\frac{4\varepsilon_i}{k_i^2-2\varepsilon_i}\right), \tag{6}$$

where

$$N_{nl}=(2\pi)^{3/2}\left[\frac{2^{4l+5}n(n-l-1)!}{\pi(n+l)!}\right]^{1/2}l!(-2\varepsilon_i)^{(2l+5)/4},$$

$\varepsilon_{i\equiv nlm}=(-Z^2/2n^2)$ and $C_{n-l-1}^{l+1}(x)$ are the normalization factor, the electron energy in the bound state of the target and the Gegenbauer polynomial, respectively. This is further simplified by expanding the Gegenbauer polynomials in terms of powers of $(k_i^2+\alpha_i)^{-1}$,

$$C_{n-l-1}^{l+1}\left(1-\frac{2\alpha_i}{k_i^2+\alpha_i}\right)=\sum_{s=0}^{n-l-1}A'_{nl,s}(k_i^2+\alpha_i)^{-s}, \tag{7}$$

in which $A'_{nl,s}$ is the expansion coefficient and $\alpha_i=-2\varepsilon_i$. Substituting Eq. (7) into Eq. (6), a convenient expanded form for $R_{nl}(k_i)$ is derived as follows:

$$R_{nl}(k_i)=\sum_{s=0}^{n-l-1}A_{nl,s}k_i^l(k_i^2+\alpha_i)^{-s-l-2}, \tag{8}$$

where $A_{nl,s}=N_{nl}A'_{nl,s}$. The radial part of the final projectile state wave function, $R_{n'l'}(k_f)$, is deduced by replacing $i$, $n$, $l$, and $m$ in Eqs. (6)–(8) with $f$, $n'$, $l'$, and $m'$, respectively. These latter expansions of the radial parts for the initial state of the target and for the final state of the projectile are substituted in Eq. (A13) and the result is

$$A_e^{(2)}=B_{lm,l'm'}\sum_{s=0}^{n-l-1}\sum_{s'=0}^{n'-l'-1}A_{nl,s}A_{n'l',s'}\times\int_0^\infty dx x^\tau e^{iax}I_{ls}^{\rho_P}(\alpha_i,x)I_{l's'}^{\rho_T}(\alpha_f,bx), \tag{9}$$

where

$$I_{ls}^{\xi}(\alpha,x)=\int_0^\infty dk k^{l+2}j_l(kx)(k^2+\alpha)^{-(l+s+2+\xi)}. \tag{10}$$

The inner integrals, $I_{ls}^{\rho_P}(\alpha_i,x)$ and $I_{l's'}^{\rho_T}(\alpha_f,bx)$, are found by evaluating the integral 10 through the following procedure. Using the integral representation of the gamma function [Eq. (A11)], we have

$$I_{ls}^{\xi}(\alpha,x)=\frac{1}{\Gamma(l+s+\xi+2)}\int_0^\infty dy y^{(l+s+1+\xi)}\times\int_0^\infty dk k^{l+2}e^{-y(k^2+\alpha)}j_l(kx). \tag{11}$$

The inner integral in the latter equation has the simple form of

$$\int_0^\infty dk k^{l+2}e^{-y(k^2+\alpha)}j_l(kx)=2^{-l-2}\pi^{1/2}x^ly^{-l-3/2}e^{-y(\alpha+x^2/4y^2)}, \tag{12}$$

which is inserted into Eq. (11) to simplify it to;

$$I_{ls}^{\xi}(\alpha,x)=\frac{2^{-l-2}\pi^{1/2}x^l}{\Gamma(l+s+\xi+2)}\int_0^\infty dy y^{s+\xi-1/2}e^{-y(\alpha+x^2/4y^2)}. \tag{13}$$

The final form of $I_{ls}^{\xi}(\alpha,x)$ is reached in terms of the Bessel functions of the third kind, $K_\nu(x)$, as;

$$I_{ls}^{\xi}(\alpha,x)=\frac{2^{-l-s-\xi-3/2}\pi^{1/2}\alpha^{-1/4(2s+2\xi+1)}}{\Gamma(l+s+\xi+2)}\times x^{l+s+\xi+1/2}K_{-s-\xi-1/2}(\sqrt{\alpha}x). \tag{14}$$

Substituting the corresponding closed forms [Eq. (14)] for the integrals, $I_{ls}^{\rho_P}(\alpha_i,x)$ and $I_{l's'}^{\rho_T}(\alpha_f,bx)$ into Eq. (9), one derives;

$$A_e^{(2)}=B_{lm,l'm'}\sum_{s=0}^{n-l-1}\sum_{s'=0}^{n'-l'-1}A_{nl,s}A_{n'l',s'}\frac{2^{-3-l-l'-s-s'-\tau}\pi\alpha_i^{-1/4(2s+2\rho_P+1)}b^{l'+s'+\rho_T+1/2}\alpha_f^{-1/4(2s'+2\rho_T+1)}}{\Gamma(l+s+\rho_P+2)\Gamma(l'+s'+\rho_T+2)}\times\int_0^{\infty}dxx^{1+l+l'+s+s'+2\tau}e^{iax}K_{-s-\rho_P-1/2}(\sqrt{\alpha_i}x)K_{-s'-\rho_T-1/2}(b\sqrt{\alpha_f}x). \tag{15}$$

Gathering all $x$-independent coefficients into expression $\mathfrak{D}_{nlmsP,n'l'm's'T}(\alpha_i,\alpha_f)$, and introducing the integral $\mathfrak{J}(\lambda,a,\kappa_P,\kappa_T,\sqrt{\alpha_i},b\sqrt{\alpha_f})$ as follows;

$$\mathfrak{J}(\lambda,a,\kappa_P,\kappa_T,\sqrt{\alpha_i},b\sqrt{\alpha_f})=\int_0^{\infty}dxx^{\lambda}e^{iax}K_{\kappa_P}(\sqrt{\alpha_i}x)K_{\kappa_T}(b\sqrt{\alpha_f}x) \tag{16}$$

gives the following simplified form of the second-order nuclear-electronic amplitude:

$$A_e^{(2)}=\sum_{s=0}^{n-l-1}\sum_{s'=0}^{n'-l'-1}\mathfrak{D}_{nlmsP,n'l'm's'T}(\alpha_i,\alpha_f)\mathfrak{J}\left(2\tau+l+l'+s+s'-1,a,-\tfrac{1}{2}-s-\rho_P,-\tfrac{1}{2}-s'-\rho_T,\sqrt{\alpha_i},b\sqrt{\alpha_f}\right). \tag{17}$$

The termination of the sums over the $s$ and $s'$ at the finite upper limits $n-l-1$ and $n'-l'-1$, respectively, assures that the amplitude is definite and single valued provided that the one-dimensional integral $\mathfrak{J}$ is finite. The one-dimensional integrals, $\mathfrak{J}$, are evaluated to give a closed-form expression for the second-order nuclear-electronic amplitude in terms of the generalized Gaussian hypergeometric functions ${}_3F_2$ and $F_4$. This has been accomplished and fully discussed by applying a symmetric impulse approximation on the amplitude [22]. One can follow the same procedure given in Ref. [22], which is valid here as well, to obtain a similar closed-form for the partial amplitude $A_e^{(2)}$. The only difference is the appearance of the pure complex variable $\tau$ as the exponent of the $x$, and $\rho_T$ and $\rho_P$ as the orders of the Bessel functions of the third kind.

### C. The first-order internuclear amplitude; $A_n^{(1)}$

The second first-order term in Eq. (3), $T_{PT}$, leads to the first-order internuclear amplitude $A_n^{(1)}$. Inserting the expansions of the radial parts of the initial and final wave functions, Eq. (8), into the integrals of Eq. (A17), the first-order internuclear amplitude is simplified as follows:

$$A_n^{(1)}=C_{1f}\sum_{s=0}^{n-l-1}A_{nl,s}\int_0^{\infty}dk_ik_i^{2+l}(k_i^2-2\varepsilon_i)^{-2-l-s+\gamma^a}+C_{1i}\sum_{s'=0}^{n'-l'-1}A_{n'l',s'}\int_0^{\infty}dk_fk_f^{2+l'}(k_f^2-2\varepsilon_f)^{-2-l'-s'+\gamma^a}. \tag{18}$$

To find the exact form of the first-order internuclear amplitude, one has to calculate the integrals, $\Upsilon_{ls}^{\xi}(\alpha)$, of the form

$$\Upsilon_{ls}^{\xi}(\alpha)=\int_0^{\infty}dkk^{l+2}(k^2+\alpha)^{-(l+s+2+\xi)}. \tag{19}$$

By introducing the integral representation of the gamma function into Eq. (19), it will reduce to

$$\Upsilon_{ls}^{\xi}(\alpha)=\frac{1}{\Gamma(l+s+\xi+2)}\int_0^{\infty}dyy^{(l+s+1+\xi)}\int_0^{\infty}dkk^{l+2}e^{-y(k^2+\alpha)}, \tag{20}$$

where the inner integral has a simple closed form given by;

$$\int_0^{\infty}dkk^{l+2}e^{-y(k^2+\alpha)}=\tfrac{1}{2}\Gamma\left(\frac{l+3}{2}\right)y^{-(l+3)/2}e^{-\alpha y}. \tag{21}$$

Substituting Eq. (21) into Eq. (20), rearranging some terms, and performing the final one-dimensional integral, yields

$$\Upsilon_{ls}^{\xi}(\alpha,x)=\frac{\Gamma\left(\frac{l+3}{2}\right)\Gamma\left(\frac{l+1}{2}+s+\xi\right)}{2\Gamma(l+s+\xi+2)\alpha^{s+\xi+(l+1)/2}}. \tag{22}$$

Thus, the final closed-form for the first-order internuclear amplitude is obtained by combining Eqs. (22), (19), and (18) as follows:

$$A_n^{(1)} = C_{1f} \sum_{s=0}^{n-l-1} A_{nl,s} \frac{\Gamma\left(\frac{l+3}{2}\right)\Gamma\left(\frac{l+1}{2}+s-\gamma^a\right)}{2\Gamma(l+s-\gamma^a+2)\alpha_i^{s-\gamma^a+(l+1)/2}} + C_{1i} \sum_{s'=0}^{n'-l'-1} A_{n'l',s'} \frac{\Gamma\left(\frac{l'+3}{2}\right)\Gamma\left(\frac{l'+1}{2}+s'-\gamma^a\right)}{2\Gamma(l'+s'-\gamma^a+2)\alpha_f^{s'-\gamma^a+(l'+1)/2}}. \tag{23}$$

### D. The second-order internuclear amplitude; $A_n^{(2a)}$

The first second-order internuclear amplitude describes another possible double-scattering mechanism. In that mechanism the projectile suffers a collision with the target nucleus and scatters at 60 degrees. This collision is followed by another target-electron collision in such a manner that the final bound system is detected at roughly sixty degrees to the forward direction for heavy targets. These subsequent collisions, in this mechanism, are described by $T$ matrices $T_{PT}$ and $T_{Te}$, respectively, while the free Green's function $G_0^{(+)}$ describes the free propagation of the system between the collisions. The general integral form of the $A_n^{(2a)}$ amplitude is given by Eq. (19) in the Appendix. Introducing the expansion for the radial parts of the wave functions, Eq. (8), into Eq. (19), generates a new simplified form for the second-order internuclear amplitude as follows:

$$A_n^{(2a)} = C_2 \sum_{s=0}^{n-l-1} A_{nl,s} \int_0^\infty dk_i k_i^{2+l} (k_i^2 - 2\varepsilon_i)^{-2-l-s+\gamma^a} \times \sum_{s'=0}^{n'-l'-1} A_{n'l',s'} \int_0^\infty dk_f k_f^{2+l'} (k_f^2 - 2\varepsilon_f)^{-2-l'-s'-\rho_T}. \tag{24}$$

The final closed-form for this partial amplitude can be obtained by combining Eqs. (19), (22), and (24) as follows:

$$A_n^{(2a)} = C_2 \sum_{s=0}^{n-l-1} A_{nl,s} \frac{\Gamma\left(\frac{l+3}{2}\right)\Gamma\left(\frac{l+1}{2}+s-\gamma^a\right)}{2\Gamma(l+s-\gamma^a+2)\alpha_i^{s-\gamma^a+(l+1)/2}} \times \sum_{s'=0}^{n'-l'-1} A_{n'l',s'} \frac{\Gamma\left(\frac{l'+3}{2}\right)\Gamma\left(\frac{l'+1}{2}+s'+\rho_T\right)}{2\Gamma(l'+s'+\rho_T+2)\alpha_f^{s'+\rho_T+(l'+1)/2}}. \tag{25}$$

### E. The second-order internuclear amplitude; $A_n^{(2b)}$

The next second-order internuclear amplitude describes a third possible double scattering mechanism, in which the projectile ejects the electron from the target. The projectile then scatters off the target nucleus into the same direction as the electron, thus forming a bound system. For heavy targets, in this case, the final pair $(P+e)$ emerges at an angle 60 degrees to the forward direction. In a quantum mechanical treatment of the process, the subsequent collisions and the free propagation of the system are described by $T$ matrices, $T_{Pe}$ and $T_{PT}$, and the Green's function $G_0^{(+)}$, respectively, although this last mechanism is not classically allowed. The amplitude, $A_n^{(2b)}$, takes a simple form, Eq. (20), which can be further simplified by introducing the expansion for the radial parts of the wave functions, Eq. (8), into it to give;

$$A_n^{(2b)} = C_3 \sum_{s=0}^{n-l-1} A_{nl,s} \int_0^\infty dk_i k_i^{2+l} (k_i^2 - 2\varepsilon_i)^{-2-l-s-\rho_P} \times \sum_{s'=0}^{n'-l'-1} A_{n'l',s'} \int_0^\infty dk_f k_f^{2+l'} (k_f^2 - 2\varepsilon_f)^{-2-l'-s'+\gamma^a}. \tag{26}$$

Once again, substituting Eqs. (19) and (22) into Eq. (26), leads us to derive the following form for the amplitude:

$$A_n^{(2b)} = C_3 \sum_{s=0}^{n-l-1} A_{nl,s} \frac{\Gamma\left(\frac{l+3}{2}\right)\Gamma\left(\frac{l+1}{2}+s+\rho_P\right)}{2\Gamma(l+s+\rho_P+2)\alpha_i^{s+\rho_P+(l+1)/2}} \times \sum_{s'=0}^{n'-l'-1} A_{n'l',s'} \frac{\Gamma\left(\frac{l'+3}{2}\right)\Gamma\left(\frac{l'+1}{2}+s'-\gamma^a\right)}{2\Gamma(l'+s'-\gamma^a+2)\alpha_f^{s'-\gamma^a+(l'+1)/2}}. \tag{27}$$

In a quantum-mechanical treatment of charge transfer each of the double scattering mechanisms, described previously, can contribute to the overall charge transfer amplitude at any angle as a result of the momentum spread of the initial and final bound states. By summing the five calculated partial amplitudes in Eqs. (5), (17), (23), (25), and (27) we find the total second-order FWL amplitude

$$A_{FWL} = A_{B1} + A_e^{(2)} + A_n^{(1)} + A_n^{(2a)} + A_n^{(2b)}. \tag{28}$$

The procedure described is applied to calculate the laboratory frame state-to-state charge transfer differential cross section from a specific initial state, $i \equiv nlm$, of the target, to the designated final state of the product, $f=n'l'm'$, in a three-body collision of an energetic ion with hydrogenlike target atoms;

$$\sigma_{nlm\to n'l'm'} = \left(\frac{d\sigma_{i\to f}}{d\Omega}\right)_{lab} = \frac{1}{4\pi^2} M_T^2 \frac{K_f}{K_i} |A_{FWL}|^2 = \frac{1}{4\pi^2} M_T^2 \frac{K_f}{K_i} |\langle f|\tau_R|i\rangle|^2, \tag{29}$$

where $\mathbf{K}_i$ and $\mathbf{K}_f$ are the initial and the final heavy-particle wave vectors in the whole-system center of mass reference frame, respectively. A simpler notation will be used to discuss the results

$$\sigma_{n'l'} = \sum_{m'=-l'}^{l'} \sigma_{100\to n'l'm'}, \tag{30}$$

since the initial state of the target is $1s$ and the spectroscopic characters replace the $l'$ values.

## IV. RESULTS AND DISCUSSION

The FWL method is now applied to calculate the state-to-state differential charge transfer cross sections for an arbitrary transition, $nlm \to n'l'm'$, in the collision of protons with atomic hydrogen. Here, charge transfer is assumed from the ground state of the atomic hydrogen target to the final bound states of the projectile up to $n=6$, where all five partial terms contribute to the transition amplitude. These calculations are restricted to incident energies of 2.8 and 5.0 MeV, corresponding to velocities 10.6 and 14.1 a.u., respectively, for which the experimental data are reported by Vogt *et al.* [19].

Figure 1 presents the differential cross sections versus the scattered angle in the laboratory frame ($\theta_{lab}$) for $1s \to 1s$, $1s \to 2s$, and $1s \to 2p$ transitions. These are denoted as $\sigma_{1s}$, $\sigma_{2s}$, and $\sigma_{2p}$, respectively, at both incident energies. The $\sigma_{2s}$ and $\sigma_{2p}$ cross sections are summed to find the differential cross sections, $\sigma_2$, for capturing into the final orbital (shell) labeled by principal quantum number $n=2$, as also shown in Fig. 1. As can be inferred from this figure, all the curves show two distinctive structures that are respectively called the "kinematic peak" and the "Thomas peak." The Thomas peak is the structure at about 0.47 mrad (as a hump or peak) and the term responsible for it is the second-order nuclear-electronic amplitude. On the other hand, the kinematic peak is quite broad and is located at more forward angles. The first Born amplitude is the most enhanced term whose main contribution is to the kinematic peak with only a negative real part and, therefore, a phase of $\pi$. Other terms in the second order FWL amplitude present different effects on these two peaks. The angular distribution of $\sigma_{2p}$ is different from those of $\sigma_{1s}$ and $\sigma_{2s}$ both in shape and magnitude, mainly due to the zero contribution of the second-order internuclear term for non-$s$-state charge transfer. The small contribution from the second-order nuclear-electronic amplitude and the angular distribution of the three degenerate final wave functions corresponding to $m=0, \pm 1$ and the complex $l$ dependence of the partial cross sections is also noted. The maximum proximity of $\sigma_{2p}$ to the $\sigma_{2s}$ occurs in a region about the Thomas angle, while the maximum discrepancy occurs in the lower and upper angular regions. Thus, the $\sigma_{2s}$ and $\sigma_2$ curves almost match everywhere except near the Thomas peak. We also note, however, that the angular distribution of $\sigma_2$ is similar to that of $\sigma_{1s}$, but smaller in magnitude.

The second-order nuclear-electronic amplitude, $A_e^{(2)}$, contributes mainly to the Thomas peak, although it has a partial destructive effect on the kinematic peak as is shown in Figs. 2 and 3. The absolute value of the second-order nuclear-electronic term, $|A_e^{(2)}|$, in the charge transfer collision of 5.0 MeV incident protons on hydrogen atoms, is plotted in Fig. 2 for the final states $1s$, $2s$, $4s$, $4p_0$, $4d_0$, $4f_0$, and $4f_2$,

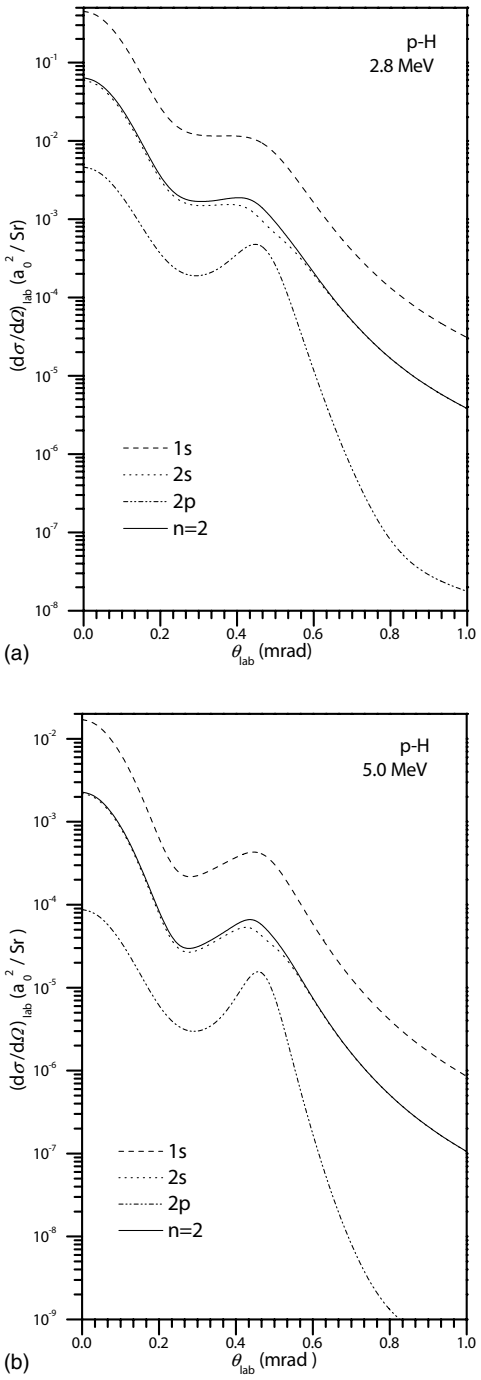


FIG. 1. The angular distribution of the state-to-state charge transfer differential cross sections in the collision of protons with hydrogen atoms, for the final states of $1s$, $2s$, $2p$, and $n=2$. Data are plotted for (a) 2.8 MeV and (b) 5.0 MeV incident energies.

where the spectroscopic notation $nl_m$ is used. In addition their corresponding phases, $\phi(A_e^{(2)})$, are plotted in Fig. 3. The absolute values and the phases of $A_e^{(2)}$ show different dependencies on quantum numbers $l$ and $m$ in the kinematic peak, Thomas peak, and at higher angles. We observe that the shape of the kinematic peak is strongly dependent on the final state wave function, ranging from two distinct structures for the final state $4f_0$ (a broad peak below 0.2 mrad and a "hump" at angles larger than 0.2 mrad) to a single hump at

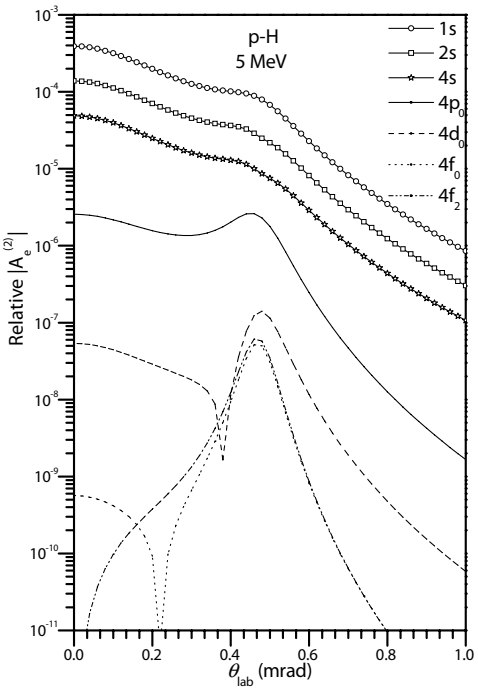


FIG. 2. The angular distribution of the absolute value of $A_e^{(2)}$ is plotted for the final states $1s$, $2s$, $4s$, $4p_0$, $4d_0$, $4f_0$, and $4f_2$. The incident energy is 5.0 MeV and this data shows the importance of the angular distribution of the final wave function on the kinematic and Thomas mechanisms.

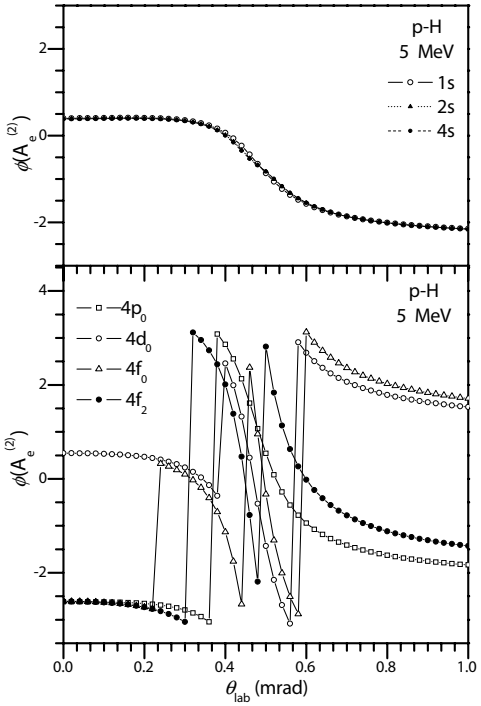


FIG. 3. The angular distribution of the relative $\phi(A_e^{(2)})$ is plotted for the final states $1s$, $2s$, $4s$, $4p_0$, $4d_0$, $4f_0$, and $4f_2$, again for the incident energy of 5.0 MeV. This data shows the constructive or destructive effect of the term on the final cross sections, $\phi(A_{B1}) = \pi$.

0.2 mrad for the final state $4f_2$, which also does not have the very forward peak otherwise apparent. The phase of the amplitudes shows the effect of this term on the final charge transfer cross section. For example, the second-order nuclear-electronic amplitude has a destructive effect on the total cross sections below the Thomas angle for the final projectile states $1s$, $2s$, $4s$, and $4d_0$ and a constructive effect at higher angles. As also shown in Fig. 3, $\phi(A_e^{(2)})$ changes once, twice or three times by a value of more than $\pi$, for the final projectile states $4p_0$, $4d_0$, and $4f_0$, respectively, about the Thomas peak.

The first-order internuclear amplitude has two terms, one of them being nonzero for the target's $s$ state and the other one being for the projectile's $s$ state. However, the second-order internuclear amplitude is only affecting the $s$-wave partial cross sections for charge transfer. Absolute values and the phases for the amplitudes of the $1s$-$1s$ transition are compared in Figs. 4 and 5, respectively. As was noted before, the first Born term dominates at forward angles with a phase of $\pi$ and thereafter decreases monotonically with scattering angle. The second-order nuclear-electronic amplitude has a kinematic peak in addition to a hump near the Thomas angle. Its phase is close to zero at forward angles and approaches to $-2$ radians at larger scattering angles (see Fig. 5). This has a destructive interference effect with the first-Born term at the kinematic peak and a partial constructive interference at larger angles. Nonetheless, the second-order nuclear-electronic term dominates over the first Born amplitude at angles higher than 0.3 mrad. The first- and the second-order internuclear terms have a phase difference of about 3.4 radians which cancel each other, but the three internuclear terms have a destructive effect on the total amplitude of the $1s$-$1s$ electron transfer amplitude in the angular range of up to 0.7 mrad. It can be seen that the second-order internuclear term dominates the first-order internuclear term over the whole range of the angular distribution and the internuclear terms are the dominant amplitude at angles higher than 0.7 mrad. This is shown in Fig. 4. Thus, the internuclear terms will contribute significantly to the total cross sections (integrated over all angles) for charge transfer.

The differential cross sections $\sigma_{3s}$, $\sigma_{3p}$, $\sigma_{3d}$, and their sum, $\sigma_3$, for 5.0 MeV bombarding energy are presented in Fig. 6. The $\sigma_{3p}$ values lie between those of $\sigma_{3s}$ and $\sigma_{3d}$, where the radial symmetry of both the initial wave function, $1s$, and the final wave function, $3s$, causes the charge transfer into the $3s$ state to be more probable than charge transfer into $3p$ and $3d$ subshells at angles below 1 mrad. This result can be generalized to all other shells described by principle quantum number $n$; i.e., charge transfer into the $s$ state of an orbital is dominant over charge transfer into all higher $l$ values. The dependence of the cross sections on $l$ values at the kinematic peak is different from those at the Thomas peak. The Thomas peak changes less with $l$ value, as compared with the kinematic peak, causing it to look "lumpier" at higher $l$ values. Nonetheless, the variation of the cross sections with the $l$ values is significant enough to cause $\sigma_3$ to be almost equal to $\sigma_{3s}$, at all angles except in the Thomas peak region. Similar features can be found for the charge transfer to final orbitals labeled by $n=4$, $n=5$, and $n=6$, although they are not plotted here to reduce the length of the manuscript.

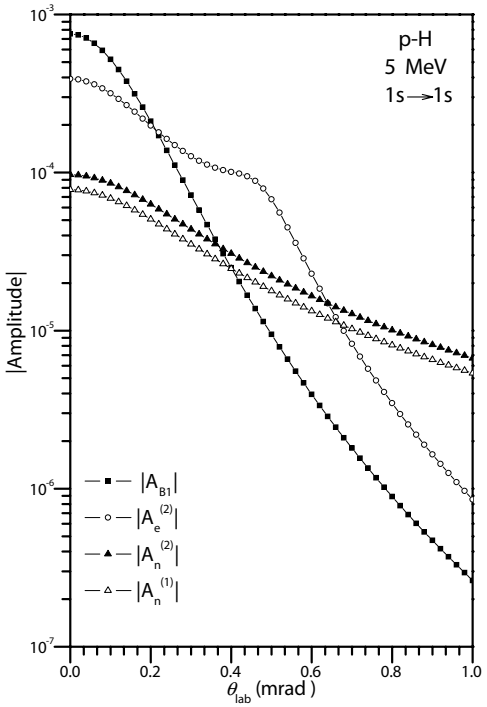


FIG. 4. The angular distribution of the absolute values of $A_{B1}$, $A_e^{(2)}$, $A_n^{(1)}$, and $A_n^{(2)}$ is plotted for the $1s \rightarrow 1s$ charge transfer mechanism in the collision of 5.0 MeV protons with hydrogen atoms. These data are plotted on a relative scale to see the importance of each term on the kinematic and Thomas peak.

In Fig. 7, differential cross sections for charge transfer from the ground state of the hydrogen target atoms to the final orbitals, $n=1$, 2, 3, 4, 5, and 6, of the final compound product are compared at the incident energy 5.0 MeV. This figure again shows the Thomas peak and the kinematic peak. The total differential charge transfer cross section, $\sigma_\Sigma$, is shown in this figure as the sum of $\sigma_1$, $\sigma_2$, $\sigma_3$, $\sigma_4$, $\sigma_5$, and $\sigma_6$. All curves are similar in shape but different in magnitude, and the differential cross sections decrease as the principal

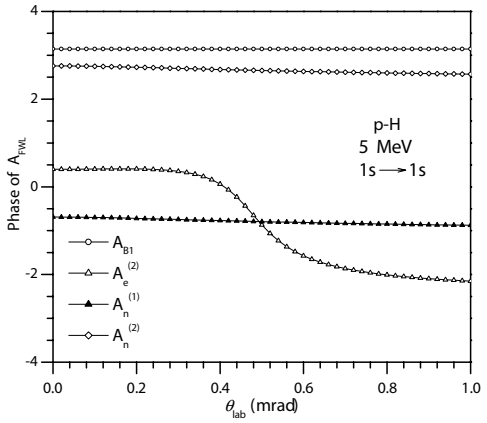


FIG. 5. The angular distribution of the phases of $A_{B1}$, $A_e^{(2)}$, $A_n^{(1)}$, and $A_n^{(2)}$ is plotted for the $1s \rightarrow 1s$ charge transfer mechanism in the collision of 5.0 MeV protons with hydrogen. This shows the constructive and destructive effect of each term on the final cross sections.

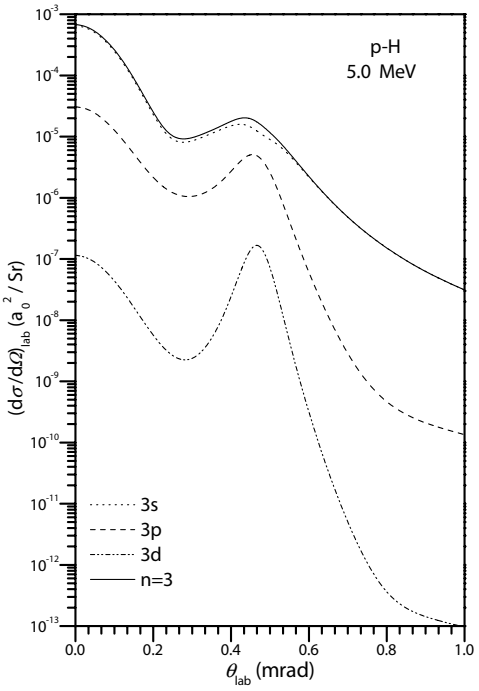


FIG. 6. The angular distribution of the state-to-state charge transfer differential cross sections in the collision of 5.0 MeV protons with hydrogen atoms for the final states of $3s$, $3p$, $3d$, and $n=3$. The $l$ dependence of the cross sections is complex.

quantum number, $n$, increases. $\sigma_{1s}$ dominates over all the other partial cross sections at all angles in the range of interest. According to $n^{-3}$ scaling rule, the all-state differential cross sections can be approximated by $\sigma_\Sigma = \Sigma_{i=1}^{n} \sigma_i + \Sigma_{i=n}^{\infty} \left(\frac{n^3}{i^3}\right) \sigma_n$ when $\sigma_i$ $(i=1,2,\ldots,n)$ are calculated. Specially, it is usual practice that the total differential cross sections summed over all the final states is estimated by means of the $n^{-3}$ scaling rule, once the result for $1s \rightarrow 1s$ transition is available. An inset is therefore presented in Fig. 7, where the quantity $n^3\sigma_n$ (for $n=1$, 3, and 5) is plotted against the scattering angle, showing that the partial cross sections can be roughly scaled by the factor $n^{-3}$. Our analysis of the proton-hydrogen collisions shows that the ratio of $\sigma_1$ and $\sigma_\Sigma$, $\sigma_\Sigma/\sigma_1$, is about 1.2 at all angles. Therefore $\sigma_1$ is approximately equal to 85 percent of the total differential cross section for transitions to all possible final bound states.

In Fig. 8, the present FWL results are compared with the available experimental measurement [19] and with results obtained from other theoretical methods such as B2F [18], CDW [3], DWB [5], and SPB [4] formalisms. The behavior over the entire range of the scattering angles can be divided into three approximate angular subregions, in which the superposition of the first- and second-order amplitudes causes dissimilar behavior in the angular distribution. The first subregion is the forward scattering region extending to the position of an interference minimum between the single and double scattering amplitudes. The second is a double scattering region centered close to the Thomas angle. The last subregion is the large scattering region in which a rapid monotonic decrease of the partial cross sections occurs. The B2F results [18] are reported to be applicable only for the first

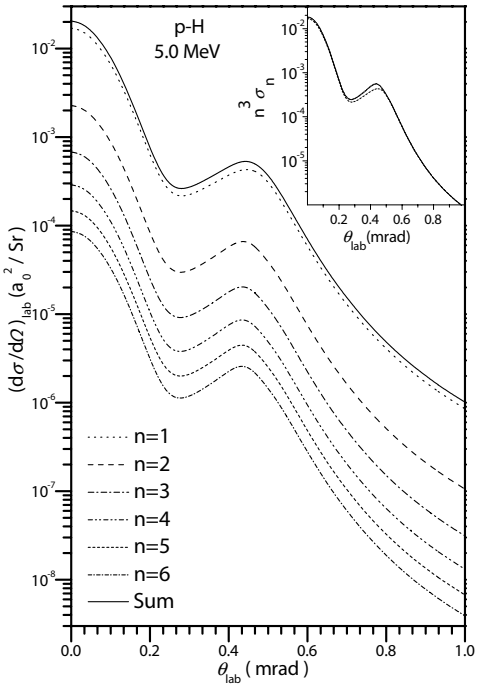


FIG. 7. The angular distribution of the state-to-state charge transfer differential cross sections in the collision of 5.0 MeV protons with hydrogen atoms, for the final states with quantum number $n=1$ to 6 and their sum. The values for $n^3\sigma_n$ are plotted against the scattering angle in the inset for $n=1$, 3, and 5, using the same representation as given in the main diagrams.

subregion of the scattering angles, up to the Thomas angle. However, even in this small angular range the FWL results are in better agreement with the experiment, as compared with the results obtained by the B2F method. Also, in this same angular region the agreement between the FWL calculation and the experimental data is better than that for the CDW, DWB, and SPB results. Figure 8 also indicates a local minimum in the angular distribution between the kinematic peak and the Thomas peak. The depth of this minimum is quite different in the different theoretical calculations, as well as for the experimental results. For an incident energy of 2.8 MeV the depth of this minimum is shallow in the case of the experimental measurements, B2F, CDW, and our FWL calculations, while the minimum is deep for the DWB and SPB cases. However, the CDW and B2F calculations fail to show a proper overall angular distribution. In the case of 5.0 MeV incident energy, this minimum is shallow only for the FWL calculations and the experimental results, it is in fact rather deep for all the other theoretical calculations. Notwithstanding this observation, the CDW and the B2F results do show a somewhat better angular distribution when compared with the experimental data. At larger scattering angles all the theory curves approach each other, but again the FWL calculations provide a better estimate of the measurements. This comparison confirms the good agreement of the FWL results with the shape and the absolute values of the angular distribution of the experiment results in all three of the angular subregions of interest.

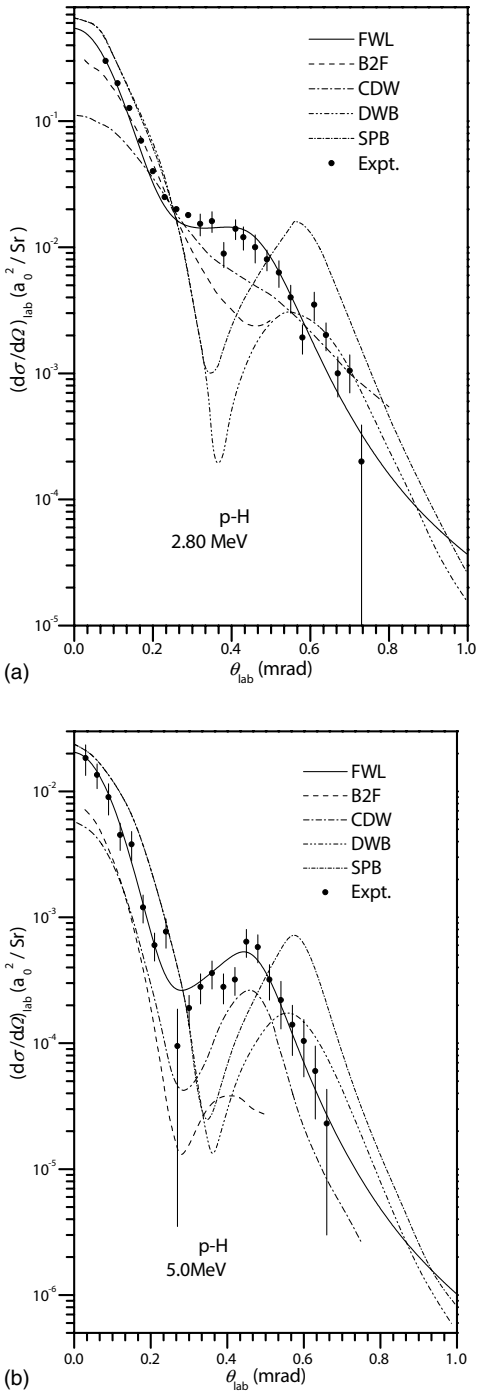


FIG. 8. The present results are compared with the available experimental data [19] and the theoretical models based on B2F [18], CDW [3], SPB [4], and DWB [5], for differential cross sections of the charge transfer from (a) 2.8 MeV and (b) 5.0 MeV protons to hydrogen atoms.

## V. CONCLUSIONS

The main goal of this investigation has been to demonstrate that the FWL three-body approach is a valuable, powerful, and yet relatively easy method for calculating the energetic ion-atom scattering processes. To this end, a calculation method based on the FWL formalism was applied

to derive the exact closed-form expressions for the differential state-to-state, $nlm \rightarrow n'l'm'$, charge exchange cross sections in collisions between an energetic projectile ion and a hydrogenlike target atom, where the final product is also assumed to be a hydrogenlike atom. We have investigated the charge transfer process in proton-hydrogen collision by means of this method as a special case. Our calculations confirm the presence of the Thomas peak in all the partial transition cross sections, and hence the importance of second-order nuclear-electronic transitions.

For transitions to a typical final orbital labeled by the principal quantum number $n$, the $s$-state transition dominates over the $p$-state transition, the $p$-transition dominates over the $d$-state transition, and so forth. The differential cross section magnitude decreases as the principal quantum number, $n$, and/or the angular momentum quantum number, $l$, increases. The $l$ dependence of the cross sections is complex. It is enhanced as the scattering angles get further from the Thomas peak, either in the forward direction or at larger angles. The $1s \rightarrow 1s$ transition dominates over all other possible final transitions, and the simple $n^{-3}$ scaling rule is also found to be valid here. The agreement of the present results with experimental data are generally good, to within the cited errors on the measurements. However, some more work is still needed for quantitative overall agreement between the absolute values of the calculated and the measured cross sections.

## ACKNOWLEDGMENTS

One of us (M.A.B.) thanks the Shahid Bahonar University, of Kerman, the Flinders University, and the Centre for Antimatter-Matter Studies for supporting his visit to the Flinders University.

## APPENDIX A

The five terms appearing in the second-order charge transfer FWL amplitudes are simplified in the momentum configuration as follows:

$$A_{B1} = \langle f|V_{Pe}|i\rangle = (2\pi)^{3/2}\varphi_i(-\mathbf{J}) \int d\mathbf{k}_f \varphi_f^*(\mathbf{k}_f) V_{Pe}(\mathbf{k}_f - \mathbf{K}), \tag{A1}$$

$$\begin{aligned} A_e^{(2)} &= \langle f|T_{Te}G_0^{(+)}T_{Pe}|i\rangle \\ &= (2\pi)^{-3} \int d\mathbf{k}_i d\mathbf{k}_f \varphi_f^*(\mathbf{k}_f)\varphi_i(\mathbf{k}_i) \\ &\quad \times T_{Te}(\mathbf{k}_f + \mathbf{v}, \mathbf{k}_i + \mathbf{k}_f - \mathbf{K}; E_f) G_0^{(+)}(E_f) \\ &\quad \times T_{Pe}(\mathbf{k}_i + \mathbf{k}_f + \mathbf{J}, \mathbf{k}_i - \mathbf{v}; E_i), \end{aligned} \tag{A2}$$

$$\begin{aligned} A_n^{(1)} &= \langle f|T_{PT}|i\rangle \\ &= \int d\mathbf{k}_i \varphi_f^*(\mathbf{k}_i - \mathbf{v})\varphi_i(\mathbf{k}_i) T_{PT}(\mu\mathbf{v} - \mathbf{k}_i - \mathbf{J}, \mu_n\mathbf{v}; E), \end{aligned} \tag{A3}$$

$$\begin{aligned} A_n^{(2a)} &= \langle f|T_{Te}G_0^{(+)}T_{PT}|i\rangle \\ &= (2\pi)^{-3} \int d\mathbf{k}_i d\mathbf{k}_f \varphi_f^*(\mathbf{k}_f)\varphi_i(\mathbf{k}_i) \times T_{Te}(\mathbf{k}_f + \mathbf{v}, \mathbf{k}_i; E_f) \\ &\quad \times G_0^{(+)}(E) T_{PT}(\mu_n\mathbf{v} + \mathbf{K} - \mathbf{k}_f, \mu_n\mathbf{v}; E), \end{aligned} \tag{A4}$$

$$\begin{aligned} A_n^{(2b)} &= \langle f|T_{PT}G_0^{(+)}T_{Pe}|i\rangle \\ &= (2\pi)^{-3} \int d\mathbf{k}_i d\mathbf{k}_f \varphi_f^*(\mathbf{k}_f)\varphi_i(\mathbf{k}_i) \times T_{PT}(\mathbf{k}_f - \mathbf{J} \\ &\quad - \mathbf{k}_i, \mu_n\mathbf{v}; E) G_0^{(+)}(E_i) T_{Pe}(\mathbf{k}_f, \mathbf{k}_i - \mathbf{v}; E_i), \end{aligned} \tag{A5}$$

where the two-body off-shell transition operators corresponding to the two-body interaction potentials $V_{PT}$, $V_{Pe}$, and $V_{Te}$ are $T_{PT}$, $T_{Pe}$, and $T_{Te}$, respectively. All other parameters in Eqs. (A1)–(A20) are defined in Table I. The partial transition amplitudes can be evaluated using the explicit forms of two-body off-the-shell $T$ matrices, the free Green's operator for the total energy, and the initial and the final wave functions. A simplified form of the modified-Coulomb two-body off-shell $T$ matrix, derived by Alston [26], is

$$T(\mathbf{k}, \mathbf{k}'; \varepsilon) = -2\pi Q(Z^a, \mathbf{k}; \varepsilon) Q(Z^a, \mathbf{k}'; \varepsilon) f_{\mathbf{k},\mathbf{k}'}(\varepsilon), \tag{A6}$$

where

$$Q(Z^a, \mathbf{k}; \varepsilon) = e^{\pi\nu^a/2}\Gamma(1 + i\nu^a)[(2\mu_n\varepsilon - k^2)/8\mu_n\varepsilon]^{-i\nu^a},$$

$$f_{\mathbf{k},\mathbf{k}'}(\varepsilon) = 2Z^e e^{2i\sigma^e}(8\mu_n\varepsilon)^{-i\nu^e}|\mathbf{k}' - \mathbf{k}|^{2i\nu^e - 2},$$

and $Z^{e(a)}$ is the effective (asymptotic) charge in the two-body modified-Coulomb potential. The free Green's operators for the total energy, in Eqs. (A2), (A4), and (A5), are, respectively, related to scattering energies by

$$G_0^{(+)}(E_f) = [E_f - (\mathbf{k}_i + \mathbf{k}_f - \mathbf{K})^2/2 + i\eta]^{-1},$$

$$G_0^{(+)}(E) = [E - (\mu_n\mathbf{v} + \mathbf{K} - \mathbf{k}_f)^2/2\mu_n + i\eta]^{-1},$$

$$G_0^{(+)}(E_i) = [E_i - k_f^2/2 + i\eta]^{-1}. \tag{A7}$$

The wave function for the initial target state in momentum space is

$$\varphi_i(\mathbf{k}_i) = R_{nl}(k_i) Y_{lm}(\hat{\mathbf{k}}_i), \tag{A8}$$

where $R_{nl}(k_i)$ and $Y_{lm}(\hat{\mathbf{k}}_i)$ are the radial and the angular (spherical harmonics) parts, spherical harmonics, respectively. In order to find the wave functions for the final projectile state in momentum space, one should replace the subscript $i$, $n$, $l$, and $m$ by $f$, $n'$, $l'$, and $m'$, respectively.

### *a. First-order Born amplitude $A_{B1}$*

It is easy to show, from Schrödinger eigenvalue equation for a two-body subsystem composed of $P$ and $e$ with interaction potential $V_{Pe}$ and energy eigenvalues $\varepsilon_f$, that the $V_{Pe}(\mathbf{k}_f - \mathbf{K})$ which appears in Eq. (A1) is equal to

$$V_{Pe}(\mathbf{k}_f - \mathbf{K}) = -(4\pi)^{3/2}\left(\frac{K^2}{\mu} - 2\varepsilon_f\right)\delta(\mathbf{k}_f - \mathbf{K}), \quad \text{(A9)}$$

in which $\mu$ is the reduced mass of the specified subsystem and is approximately equal to 1 a.u. for hydrogen atoms. Inserting this expression into Eq. (A1) and integrating over the three-dimensional Dirac delta function leads to Eq. (5).

### b. Second-order amplitude $A_e^{(2)}$

Substituting the two-body $T$ matrices from Eq. (A6) into Eq. (A2), the second-order amplitude $A_e^{(2)}$ becomes;

$$A_e^{(2)} = B\int d\mathbf{k}_i d\mathbf{k}_f \varphi_f^*(\mathbf{k}_f)\varphi_i(\mathbf{k}_i)(k_i^2 - 2\varepsilon_i)^{-\rho_P}(k_f^2 - 2\varepsilon_f)^{-\rho_T}(\zeta + 2\mathbf{k}_i\cdot\mathbf{K} - 2\mathbf{k}_f\cdot\mathbf{J} + i\eta)^{-1-\tau}, \quad \text{(A10)}$$

where $B$ is defined;

$$B = \left(\frac{4}{\pi}\right)2^{\tau}Z_P Z_T e^{i\pi\tau}\frac{\Gamma(1+\rho_P)^2\Gamma(1-\delta_P)}{\Gamma(1+\delta_P)} \times \frac{\Gamma(1+\rho_T)^2\Gamma(1-\delta_T)}{\Gamma(1+\delta_T)} \times (4\mathbf{v}^2)^{2\tau-\delta_P-\delta_T} J^{-2+2\delta_P} K^{-2+2\delta_T}.$$

All the parameters are given in Table I. The six-dimensional integral in Eq. (A10) has three brunch cuts in the complex plane due to the presence of factors with noninteger exponents. To avoid the cut lines and simplify the computations, one introduces the integral representation [27]:

$$\beta^{-1-\tau} = \frac{1}{\Gamma(1+\tau)} \times \int_0^\infty dx x^{\tau} e^{-\beta x}; \quad \text{(A11)}$$

$$\mathrm{Re}(\beta) > 0,$$

$$\mathrm{Re}(\tau) > -1),$$

into Eq. (A10) and therefore simplifying Eq. (A10) further as follows:

$$A_e^{(2)} = B\frac{\exp[-i(1+\tau)\pi/2]}{\Gamma(1+\tau)}\int_0^\infty dx x^{\tau} \times \int d\mathbf{k}_i \varphi_i(k_i)(k_i^2 - 2\varepsilon_i)^{-\rho_P} e^{2i\mathbf{k}_i\cdot\mathbf{K}x} \times \int d\mathbf{k}_f \varphi_f^*(k_f)(k_f^2 - 2\varepsilon_f)^{-\rho_T} e^{-2i\mathbf{k}_f\cdot\mathbf{J}x}. \quad \text{(A12)}$$

This is further simplified by a proper expansion of the exponents in the second and third integrals and integration over the angular parts of the momentums $\mathbf{k}_i$ and $\mathbf{k}_f$. The result is

$$A_e^{(2)} = B_{lm,l'm'}\int_0^\infty dx x^{\tau} e^{iax}\int_0^\infty dk_i k_i^2 R_{nl}(k_i) j_l(k_i x)(k_i^2 - 2\varepsilon_i)^{-\rho_P} \times \int_0^\infty dk_f k_f^2 R_{n'l'}(k_f) j_l(bk_f x)(k_f^2 - 2\varepsilon_f)^{-\rho_T}, \quad \text{(A13)}$$

where

$$B_{lm,l'm'} = (4\pi)^2 i^{l-l'}(2K)^{-1-\tau} \times \frac{\exp[-i(1+\tau)\pi/2]}{\Gamma(1+\tau)} \times Y_{lm}(\hat{\mathbf{K}})Y_{l'm'}^*(\hat{\mathbf{J}}) \times \mathrm{B}. \quad \text{(A14)}$$

### c. First-order amplitude $A_n^{(1)}$

By introducing appropriate two-body $T$-matrices from Eq. (A6), the first-order internuclear amplitude reduces to

$$A_n^{(1)} = B'\int d\mathbf{k}_\mathbf{i}\varphi_f^*(\mathbf{k}_\mathbf{i} - \mathbf{v})\varphi_i(\mathbf{k}_\mathbf{i})|\mathbf{k}_\mathbf{i} + \mathbf{J}|^{-2-2\gamma}, \{[(\mathbf{k}_i - \mathbf{v})^2 - 2\varepsilon_f](k_i^2 - 2\varepsilon_i)\}^{\gamma^a}, \quad \text{(A15)}$$

where

$$B' = 4\pi Z_P Z_T e^{i\pi\gamma^a}\frac{\Gamma(1-\gamma^a)^2\Gamma(1+\gamma)}{\Gamma(1-\gamma)}(4\mu_n\mathbf{v}^2)^{\gamma-2\gamma^a}.$$

The integrand in Eq. (A15) has two local maxima at $\mathbf{k}_i$ approximately equal to 0 and $\mathbf{v}$. Since the two maxima are well separated in momentum space, the integrand is expanded into two terms. Then, the first-order internuclear amplitude would be simplified as follows:

$$A_n^{(1)} = (4\pi)^{1/2}B' \times \left[J^{-2-2\gamma}(\mathbf{v}^2 - 2\varepsilon_f)^{\gamma^a}\varphi_f^*(-\mathbf{v})\delta_{l0}\delta_{m0} \times \int_0^\infty dk_i k_i^2 R_{nl}(k_i)(k_i^2 - 2\varepsilon_i)^{\gamma^a} + K^{-2-2\gamma}(\mathbf{v}^2 - 2\varepsilon_i)^{\gamma^a}\varphi_i(\mathbf{v})\delta_{l'0}\delta_{m'0}\int_0^\infty dk_f k_f^2 R_{n'l'}(k_f)(k_f^2 - 2\varepsilon_f)^{\gamma^a}\right]. \quad \text{(A16)}$$

The coefficients of the integrals are changed to single parameters:

$$C_{1f} = (4\pi)^{1/2}B'J^{-2-2\gamma}(\mathbf{v}^2 - 2\varepsilon_f)^{\gamma^a}\varphi_f^*(-\mathbf{v})\delta_{l0}\delta_{m0}$$

and

$$C_{1i} = (4\pi)^{1/2}B'K^{-2-2\gamma}(\mathbf{v}^2 - 2\varepsilon_i)^{\gamma^a}\varphi_i(\mathbf{v})\delta_{l'0}\delta_{m'0}$$

and the first-order internuclear amplitude is simplified as follows:

$$A_n^{(1)} = C_{1f}\int_0^\infty dk_i k_i^2 R_{nl}(k_i)(k_i^2 - 2\varepsilon_i)^{\gamma^a} + C_{1i}\int_0^\infty dk_f k_f^2 R_{n'l'}(k_f) \times (k_f^2 - 2\varepsilon_f)^{\gamma^a}. \quad \text{(A17)}$$

### d. Second-order amplitude $A_n^{(2a)}$

The following expression can be derived, by substituting the proper two-body $T$ matrices from Eq. (A6) into Eq. (A4), for the first of second-order terms in the internuclear amplitude;

$$A_n^{(2a)} = C_2' \int d\mathbf{k}_i d\mathbf{k}_f \varphi_f^*(\mathbf{k}_f)\varphi_i(\mathbf{k}_i)(k_i^2 - 2\varepsilon_i)^{\gamma^a}(k_f^2 - 2\varepsilon_f)^{\rho_T}, \tag{A18}$$

for

$$\begin{aligned} C_2' = &-\left(\frac{2}{\pi}\right) Z_P Z_T^2 e^{i\pi(\gamma^a - \rho_T)} \times \frac{\Gamma(1-\gamma^a)^2\Gamma(1+\gamma)}{\Gamma(1-\gamma)} \\ &\times \frac{\Gamma(1-\rho_T)^2\Gamma(1+\delta_T)}{\Gamma(1-\delta_T)} \\ &\times (4\mu_n \mathbf{v}^2)^{\gamma - 2\gamma^a}(2\mathbf{v})^{2(2\rho_T - \delta_T)}\mathbf{v}^{2\delta_T - 2} \\ &\times \left(\frac{1}{2}\mathbf{v}^2 + \varepsilon_f\right)^{\gamma^a - \rho_T - 1} K^{-2-2\gamma}. \end{aligned}$$

This term is further simplified by inserting the hydrogenic wave functions into it, and evaluating the angular integrals as follows:

$$\begin{aligned} A_n^{(2a)} = C_2 &\int_0^\infty dk_i k_i^2 R_{n'l'}(k_i)(k_i^2 - 2\varepsilon_i)^{\gamma^a} \\ &\times \int_0^\infty dk_f k_f^2 R_{nl}(k_f)(k_f^2 - 2\varepsilon_f)^{-\rho_T}, \end{aligned} \tag{A19}$$

with $C_2 = 4C_2'\delta_{l'0}\delta_{m'0}\delta_{l0}\delta_{m0}$.

### *e. Second-order amplitude* $A_n^{(2b)}$

Similarly, for the second of the second-order terms in the internuclear amplitude from Eq. (A5), one finds

$$\begin{aligned} A_n^{(2b)} = C_3 &\int_0^\infty dk_i k_i^2 R_{nl}(k_i)(k_i^2 - 2\varepsilon_i)^{-\rho_P} \\ &\times \int_0^\infty dk_f k_f^2 R_{n'l'}(k_f)(k_f^2 - 2\varepsilon_f)^{\gamma^a}, \end{aligned} \tag{A20}$$

where

$$\begin{aligned} C_3 = &-4\left(\frac{2}{\pi}\right) Z_P^2 Z_T e^{i\pi(\gamma^a - \rho_P)} \frac{\Gamma(1-\gamma^a)^2\Gamma(1+\gamma)}{\Gamma(1-\gamma)} \\ &\times \frac{\Gamma(1+\rho_P)^2\Gamma(1-\delta_P)}{\Gamma(1+\delta_P)} \\ &\times (4\mu_n \mathbf{v}^2)^{\gamma - 2\gamma^a}(2\mathbf{v})^{2(2\rho_P - \delta_P)}\mathbf{v}^{2\delta_P - 2} \\ &\times \left(\frac{1}{2}\mathbf{v}^2 + \varepsilon_f\right)^{\gamma^a - \rho_P - 1} J^{-2-2\gamma}\delta_{l'0}\delta_{m'0}\delta_{l0}\delta_{m0}. \end{aligned}$$


[1] L. H. Toburen, Radiat. Environ. Biophys. **37**, 221 (1998).
[2] M. Biaggum, F. Ballarini, W. Burkard, E. Egger, A. Ferrari, and A. Ottolenghi, Nucl. Instrum. Methods Phys. Res. B **159**, 89 (1999).
[3] H. F. Busnengo, A. E. Martinez, R. D. Rivarola, and L. J. Dube, J. Phys. B **28**, 3283 (1995).
[4] J. Macek and S. Alston, Phys. Rev. A **26**, 250 (1982); S. Alston, *ibid.* **38**, 3124 (1988).
[5] K. Taulbjerg and J. S. Briggs, J. Phys. B **16**, 3811 (1983).
[6] Dz. Belkic, S. Saini, and H. S. Taylor, Phys. Rev. A **36**, 1601 (1987).
[7] D. P. Dewangan and B. H. Bransden J. Phys. B **21**, L353 (1988).
[8] D. P. Dewangan and J. Eichler, Phys. Rep. **247**, 59 (1994).
[9] L. D. Faddeev, Sov. Phys. JETP **12**, 1014 (1961).
[10] K. M. Watson, Phys. Rev. **88**, 1163 (1952).
[11] C. Lovelace, Phys. Rev. B **135**, 1225 (1964).
[12] As examples see; E. O. Alt, G. V. Avokov, L. D. Blokhintsev, A. S. Kadyrov, and A. M. Mukhmedzhanov, J. Phys. B **27**, 4652 (1994); A. M. Veselova, Teor. Mat. Fiz. **35**, 180 (1978); A. M. Veselova, *ibid.* **3**, 326 (1970); S. P. Merkurev, Sov. J. Nucl. Phys. **24**, 150 (1976).
[13] S. Alston, Nucl. Instrum. Methods Phys. Res. B **43**, 19 (1989).
[14] S. Alston, Phys. Rev. A **40**, 4907 (1989).
[15] S. Alston, Phys. Rev. A **42**, 331 (1990).
[16] E. O. Alt, A. S. Kadyrov, and A. M. Mukhamedzhanov, Phys. Rev. A **60**, 314 (1999).
[17] E. Ghanbari Adivi and M. A. Bolorizadeh, J. Phys. B **37**, 3321 (2004).
[18] P. S. Vinitsky, Yu. V. Popov, and O. Chuluunbaatar, Phys. Rev. A **71**, 012706 (2005).
[19] H. Vogt, R. Schuch, E. Justiniano, M. Schulz, and W. Schwab, Phys. Rev. Lett. **57**, 2256 (1986).
[20] P. J. Martin, D. M. Blankenship, T. J. Kvale, E. Redd, J. L. Peacher, and J. T. Park, Phys. Rev. A **23**, 3357 (1981).
[21] K. Dettmann in, Springer Tracts Mod. Phys. **58**, 119 (1971).
[22] E. Ghanbari Adivi and M. A. Bolorizadeh, Few-Body Syst. **39**, 11 (2006).
[23] G. R. Newton, *Scattering Theory of Waves and Particles*, (Springer, New York, 1982).
[24] J. C. Y. Chen, in: Case Stud. At. Phys. **3**, 305 (1974).
[25] C. J. Joachain, *Quantum Collision Theory*, (North-Holland, Amsterdam, 1987).
[26] S. Alston, Phys. Rev. A **38**, 636 (1988).
[27] I. S. Gradshteyn and I. M. Ryzhik, *Tables of Integrals, Series and Products*, (Academic Press, New York, 1980).